PERGAMON

International Journal of Heat and Mass Transfer 44 (2001) 3081–3093

International Journal of HEAT and MASS TRANSFER

www.elsevier.com/locate/ijhmt

Gas-phase unsteadiness and its influence on droplet vaporization in sub- and super-critical environments

Guang-Sheng Zhu [a,1], Rolf D. Reitz [a,*], Suresh K. Aggarwal [b,2]

[a] *Engine Research Center, University of Wisconsin, Madison, 1500 Engineering Drive, Madison, WI 53706, USA*

[b] *Department of Mechanical Engineering, University of Illinois, Chicago, 842 W. Taylor St., RM 2039, Chicago, IL 60607, USA*

Received 18 February 2000; received in revised form 23 October 2000

Abstract

This paper aims to investigate quantitatively the influence of gas-phase unsteadiness on the droplet vaporization process in sub- and super-critical environments. Two comprehensive models of high-pressure droplet vaporization, including a transient model and another assuming gas-phase quasi-steadiness, are presented. Both models are first compared with experimental data and then used to calculate vaporization processes of single droplets of different initial sizes for environmental conditions in which the ambient pressure and temperature range from 1–150 atm and 500–2000 K, respectively. The unsteady effects are quantified by introducing characteristic time scale ratios. It is shown that strong gas-phase unsteadiness exists during the early period of the vaporization process. The unsteadiness attains a maximum value in the gas near the droplet surface and decreases quickly to a nearly steady value within a short distance from the surface. With increasing ambient pressure, the unsteadiness increases nearly linearly at low ambient temperatures and rapidly at high ambient temperature. Gas-phase unsteadiness also increases with increasing ambient temperature and is affected even more strongly by temperature. Compared to the transient model, the quasi-steady model predicts a smaller regression rate initially and a larger regression rate during the later period. The differences between the predicted regression rates, and thus between the predicted vaporization processes, are magnified with increasing ambient temperatures and/or pressures. The vaporization process predicted using the quasi-steady model reaches the critical mixing state earlier than that predicted using the transient model. These conclusions also apply for the vaporization processes of single droplets of different initial sizes.

1. Introduction

Theoretical research of spray vaporization and combustion processes of practical liquid-fueled engines often require calculations of the vaporization rates of many individual droplets. The predictions of important engine characteristics such as fuel economy and pollutant emissions rely significantly on the accuracy of the droplet vaporization model. During the past several decades, many models have been studied extensively. Descriptions of these models can be found in the reviews of Williams [1], Law [2], Sirignano [3], Peng and Aggarwal [4], and Givler and Abraham [5].

Various droplet vaporization models, including classical low-pressure models [1–4,6,7] and those incorporating high-pressure effects [8], are currently employed in practical applications [8,9]. A general feature of these models is that they assume gas-phase quasi-steadiness, an assumption that has attracted much interest [1–5,10–12]. The assumption is based on the argument that the gas-phase transport rate is much faster than the rate at which the properties at droplet surface change due to the significant disparity between the gas and liquid densities. Matalon and Law [11] further derived the result that the gas-phase unsteadiness leads to a change of relative order $O[(\rho_g/\rho_l)^{1/2}]$ in the droplet vaporization rate. Wong et al. [12] also indicated that the gas-phase unsteadiness

* Corresponding author. Tel.: +1-608-262-0145; fax: +1-608-262-6707.

E-mail addresses: zhugs@erc.wisc.edu (G.-S. Zhu), reitz@engr.wisc.edu (R.D. Reitz), ska@uic.edu (S.K. Aggarwal).

[1] Tel.: +1-608-265-6432; fax: +1-608-262-6707.

[2] Tel.: +1-312-996-2235; fax: +1-312-413-0447.

0017-9310/01/$ - see front matter
PII: S0017-9310(00)00349-5

is an important consideration in order to correctly predict droplet ignition. However, all of these studies are based on models that are essentially only suitable for low-pressure conditions.

For the droplet vaporizing under high-pressure conditions, the vaporization process has many important aspects that are not adequately considered by low-pressure models. For example, the phase equilibrium at the droplet surface can no longer be represented by a Clausius–Clapeyron-type equation [5]. Also the solubility of gases into the liquid significantly alters the liquid properties and thus the droplet vaporization behavior [5,13]. Another consideration is that the liquid- and gas-phase thermophysical properties become pressure-dependent. As the droplet surface approaches the critical state, high-pressure effects and transcritical phenomena become extremely important. As a consequence, the high-pressure vaporization process exhibits significantly different characteristics from those predicted with low-pressure models [5,8,13–15]. Therefore, for droplet high-pressure vaporization, conclusions derived with a low-pressure model may not be applicable, and the gas-phase unsteadiness and its influence need to be examined further. In practical applications droplet vaporization/combustion processes generally occur at conditions of high pressure and temperature that typically exceed the critical pressure and temperature of the fuel by a factor of two or more. In order to validate the reliability of quasi-steady vaporization models, it is also necessary to clarify the gas-phase unsteadiness behavior and its influence under high-pressure conditions.

The objective of the present study was to investigate quantitatively the effect of gas-phase unsteadiness on the droplet vaporization process, over a range of ambient pressure and temperature conditions which include both sub- and super-critical conditions. This range covers most of the conditions in which practical droplets and sprays evaporate. A transient and a quasi-steady vaporization model are presented and validated against available experimental data. The gas-phase unsteadiness of the transient process and its influence on the vaporization process are analyzed.

2. Physical model

The physical model considers a droplet that is initially at a sub-critical state and introduced into a stagnant gas environment whose thermodynamic state is varied to include both the sub-critical and super-critical regimes of the fuel. Radiation and second-order effects such as the Soret and Dufour effects are assumed to be negligible. A spherically symmetric vaporization process is assumed. The governing equations for both the gas- and liquid-phases and the interphase conditions at the droplet surface are described as follows:

2.1. Governing equations

For the transient model, the governing equations in the gas-phase region, $r > r_s(t)$, are [14]:

$$\frac{\partial \rho_k}{\partial t} + \frac{1}{r^2}\frac{\partial}{\partial r}(\rho_k u r^2) = \frac{1}{r^2}\frac{\partial}{\partial r}\left[\rho D_k r^2 \frac{\partial}{\partial r}\left(\frac{\rho_k}{\rho}\right)\right], \tag{1}$$

$$\frac{\partial \rho u}{\partial t} + \frac{1}{r^2}\frac{\partial}{\partial r}\left(\rho u^2 r^2\right) + \frac{\partial p}{\partial r} = \frac{1}{r^2}\frac{\partial}{\partial r}\left[2\mu r^2 \frac{\partial u}{\partial r} + \lambda \frac{\partial}{\partial r}(ur^2)\right] - \frac{2}{r^2}\left[2\mu u + \frac{\lambda}{r}\frac{\partial}{\partial r}(ur^2)\right], \tag{2}$$

$$\frac{\partial \rho I}{\partial t} + \frac{1}{r^2}\frac{\partial}{\partial r}(\rho I u r^2) + \frac{p}{r^2}\frac{\partial}{\partial r}(ur^2) = \frac{1}{r^2}\left\{\frac{\partial}{\partial r} r^2 \rho D_k \left[\sum_{k=1}^{N} h_k \frac{\partial}{\partial r}\left(\frac{\rho_k}{\rho}\right)\right]\right\} + \frac{1}{r^2} \times \frac{\partial}{\partial r}\left(\alpha r^2 \frac{\partial T}{\partial r}\right) + \frac{\partial u}{\partial r}\left[2\mu \frac{\partial u}{\partial r} + \frac{\lambda}{r^2}\frac{\partial}{\partial r}(ur^2)\right] + \frac{2u}{r^2}\left[2\mu u + \frac{\lambda}{r}\frac{\partial}{\partial r}(ur^2)\right], \tag{3}$$

$$f_1(p, T, \rho_1, \rho_2, \ldots, \rho_N) = 0, \tag{4}$$

where t refers to time and r is the spatial variable. u, p, T, I and ρ are the mass-averaged velocity, pressure, temperature, specific internal energy and the density of the mixture, respectively. $r_s(t)$ is the instantaneous droplet radius, and D_k, ρ_k and h_k are the diffusion coefficient, density and specific enthalpy of kth species, respectively. N is the total number of species. Further, α, μ, and λ are the thermal conductivity, viscosity, and second viscosity coefficient, respectively. Eqs. (1)–(3) represent the conservation of species mass, mixture momentum and energy, while Eq. (4) represents the equation of state (EOS) in a generalized form. A cubic EOS is employed to represent the nonideal gas behavior that can be written as [16]:

$$p = \frac{RT}{V - b} - \frac{a}{V^2 + qbV + wb^2}, \tag{5}$$

where parameters a and b are functions of species properties and ambient conditions obtained via mixing rules with their corresponding values for each discrete species [16]. The values of the constants q and w depend on the particular EOS employed. Three most commonly used EOS are the Redlich-Kwong (RK), and the Soave–Redlich–Kwong, and the Peng–Robinson (PR) EOS. In a previous study [14], the capabilities of these EOS for predicting the phase equilibrium and the transcritical droplet vaporization behavior were rigorously examined. Predictions using the PR-EOS were found to be in excellent agreement with experimental data over a wide range of ambient pressures, while those using the RK-

EOS displayed significant differences. Consequently, the PR-EOS is employed in the present study. The values of q and w for PR-EOS are $q = 2$, $w = -1$.

The gas-phase equations for the quasi-steady model can be extracted by simply dropping the unsteady term in Eqs. (1)–(3). If we further neglect the viscous effect and the pressure variation in the flow field, the quasi-steady form of the gas-phase equations can be written as:

$$\rho u r^2 = M = \text{const.}, \tag{6}$$

$$M\frac{\partial}{\partial r}\left(\frac{\rho_k}{\rho}\right) = \frac{\partial}{\partial r}\left[\rho D_k r^2 \frac{\partial}{\partial r}\left(\frac{\rho_k}{\rho}\right)\right], \tag{7}$$

$$M\frac{\partial I}{\partial r} = \frac{\partial}{\partial r}\left\{r^2 \rho D_k \left[\sum_{k=1}^{N} h_k \frac{\partial}{\partial r}\left(\frac{\rho_k}{\rho}\right)\right]\right\} + \frac{\partial}{\partial r^2}\left(\alpha r^2 \frac{\partial T}{\partial r}\right). \tag{8}$$

Mathematically speaking, Eqs. (6)–(8) are the results of Eqs. (1)–(3) for the same boundary conditions when the process time is infinite, or, when the gas-phase transport rates become infinitely fast.

The liquid-phase transport inside the droplet is considered to be time- and space-dependent for both the quasi-steady and the transient gas-phase models. The diffusion limit model is employed. Then, for the liquid-phase, $r < r_s$, the governing equations are the energy and species equations:

$$\frac{\partial}{\partial t}(\rho_l C_{pl} T_l) = \frac{1}{r^2}\frac{\partial}{\partial r}\left(\alpha_l r^2 \frac{\partial T_l}{\partial r}\right) + \frac{1}{r^2} \times \frac{\partial}{\partial r}\left[r^2 \sum_{k=1}^{N} \rho_l D_l h_k \frac{\partial}{\partial r}\left(\frac{\rho_{lk}}{\rho_l}\right)\right], \tag{9}$$

$$\frac{\partial \rho_{lk}}{\partial t} = \frac{1}{r^2}\frac{\partial}{\partial r}\left[\rho_l D_l r^2 \frac{\partial}{\partial r}\left(\frac{\rho_{lk}}{\rho_l}\right)\right], \tag{10}$$

where the subscript l denotes the liquid phase, and C_p is the specific heat at constant pressure.

2.2. Boundary conditions

At the droplet surface, $r = r_s$, the conditions of mass and energy conservation, and thermodynamic equilibrium are represented as:

$$\dot{m}X_k - \rho_l D_l \frac{\partial X_k}{\partial r}\bigg|_{r=r_s^-} = \dot{m}Y_k - \rho D_k \frac{\partial Y_k}{\partial r}\bigg|_{r=r_s^+}, \tag{11}$$

$$-\alpha_l \frac{\partial T_l}{\partial r}\bigg|_{r=r_s^-} = -\alpha \frac{\partial T}{\partial r}\bigg|_{r=r_s^+} + \sum_{k=1}^{N}\left(\dot{m}Y_k - \rho D_k \frac{\partial Y_k}{\partial r}\right)\bigg|_{r=r_s^+} \Delta H_{vk}, \tag{12}$$

$$f_2(T_s, P_s, X_{1s}, X_{2s}, \ldots, X_{Ns}, Y_{1s}, Y_{2s}, \ldots, Y_{Ns}) = 0, \tag{13}$$

where $\dot{m}$ is the droplet gasification rate, and X_{is} and Y_{is} represent, respectively, the liquid- and gas-phase mole fractions of ith species at the droplet surface. The specific form of Eq. (13) can be derived from the condition of thermodynamic and mechanical equilibrium at the droplet surface. At low pressures the equilibrium is normally expressed by Raoult's law. However, at elevated pressures it should be described from more general thermodynamic considerations, as discussed in Section 2.3. The boundary conditions at the droplet center ($r = 0$) are: $\partial T_l/\partial r = 0$ and $\partial \rho_{lk}/\partial r = 0$, and those at $r \to \infty$ are: $T \to T_\infty, p \to p_\infty$, and $\rho_k \to \rho_{k\infty}$.

In a super-critical environment, depending on the ambient and droplet properties, the droplet may experience a thermodynamic state transition from sub- to super-critical. Eqs. (10)–(13) are only applicable until the droplet surface reaches a critical mixing point. At the critical mixing point, the droplet surface becomes indistinguishable from the gas phase. The subsequent droplet regression is then characterized by the motion of the critical surface that moves inward continuously. This is an important feature of the present models. With this treatment, the droplet regression process can also be handled even after the droplet surface reaches the critical state, whereas most of the other high-pressure models stop the calculation at the time when the surface reaches the critical state [5].

2.3. Vapor–liquid equilibrium at the droplet surface

When the droplet surface is in mechanical and thermodynamic equilibrium, the temperature, pressure, and fugacity of each species in the gas-phase is equal to the corresponding property of the same species in the liquid-phase. The equality of fugacity of species k is expressed as:

$$\phi_k {}^{v}Y_k = \phi_k {}^{l}X_k \tag{14}$$

where the superscripts v and l refer to the vapor- and liquid-phase, respectively. ϕ_k is the fugacity coefficient of the kth species, and is a function of pressure, temperature, and composition. It is given in terms of the volumetric properties of the mixture by the following thermodynamic relation [16]:

$$RT\ln(\phi_k) = \int_v^\infty \left[\left(\frac{\partial P}{\partial n_k}\right)_{T,v,n_j} - \frac{RT}{v}\right] dv - RT\ln z, \tag{15}$$

where z is the compressibility factor, and n_j is the mole number of jth species. By substituting the equation of state (5) into Eq. (15), the fugacity of the kth species in the liquid- and gas-phase mixture is given by [16]:

$$\ln\phi_k = \frac{b_k}{b}(z-1) - \ln(z-B) + \frac{A}{B\sqrt{q^2-4w}}\left(\frac{b_k}{b} - \delta_k\right) \times \ln\left(\frac{2z+B(q+\sqrt{q^2-4w})}{2z+B(q-\sqrt{q^2-4w})}\right), \quad (16)$$

where

$$\frac{b_k}{b} = \frac{T_{ck}/P_{ck}}{\sum_j y_j T_{cj}/P_{cj}}, \quad \delta_k = \frac{2\sqrt{a_k}}{a}\sum x_j\sqrt{a_j}(1-k_{kj}).$$

The binary interaction coefficient k_{kj} in the above equation is taken from Knapp et al. [28]. It is 0.1441 for PR-EOS for the *n*-heptane-nitrogen system. Eqs. (14)–(16) provide the basic relations for the vapor–liquid equilibrium calculation. These equations along with Eqs. (11) and (12) provide a closed system to determine the temperature and species mole fractions at the droplet surface. It represents a system of highly nonlinear algebraic equations that need to be solved iteratively at each time step.

For a multicomponent mixture, the energy required for phase change for each species is defined as the difference between the partial molar enthalpy of that species in the vapor- and liquid-phases. The following thermodynamic relation then gives the partial molar enthalpy of *k*th species:

$$\bar{H}_k - \bar{H}_k^0 = -RT^2\frac{\partial}{\partial T}(\ln\phi_k) \quad (17)$$

where the superscript 0 denotes the quantity in an ideal state. Eq. (17) is solved iteratively along with Eqs. (11) and (12) and (14)–(16).

2.4. Thermophysical properties

The gas- and liquid-phase thermodynamic and transport properties are functions of pressure, temperature and composition. The method reported by Chung [18,19] is employed to calculate the thermal conductivity and viscosity of the gas mixture at high pressures. The binary mass diffusivity is calculated by means of the Chapman–Enskog theory in conjunction with the collision integrals given by Neufeld [20]. It is then corrected for pressure effects by using the Takahashi correlation [21]. For a multicomponent mixture, the effective diffusivity is obtained by using the formula given by Bird et al. [22]. For the enthalpy of the gas mixture, the enthalpy of the pure components is obtained from the JANAF tables. A generalized thermodynamic correlation based on three-parameter corresponding states [23] is then used to calculate the enthalpy correction for high-pressure effects. Then, the specific internal energy of the gas mixture in Eq. (3) is given by:

$$I = \sum_{k=1}^{N}\frac{\rho_k}{\rho}h_k(T) - \frac{p}{\rho} \quad (18)$$

which relates the energy Eq. (3) to the equation of state (4) through the gas temperature.

The heat capacity of pure liquid components is calculated by a fourth-order polynomial of temperature, and is then extended to liquid mixtures using the mixture rule of Filippov [24,25]. The liquid mass diffusivity and thermal conductivity are obtained by using the correlations of Nakanishi [26] and Chung [18], respectively. The liquid density is obtained directly from the EOS.

2.5. Numerical method

An arbitrary Lagrangian–Eulerian numerical method with a dynamically adaptive mesh was used to solve the transient gas-phase equations. The solution procedure is as follows: (1) calculate explicitly the contributions of the diffusion and source terms in the gas-phase equations; (2) calculate implicitly the terms associated with the acoustic pressure in the gas-phase equations; (3) compute a new mesh distribution with the adaptive mesh method, and then calculate the convection terms in the gas-phase equations; and (4) based on the solutions of the above steps, solve implicitly the liquid-phase equations as well as the droplet surface and vapor–liquid equilibrium equations. The radial coordinate of the adaptive mesh is calculated using the formula given in Zhu and Aggarwal [14].

The quasi-steady gas-phase and the transient liquid-phase equations are discretized using a finite control volume approach. The discretized equations are solved by using the TriDiagonal-Matrix Algorithm (TDMA) methodology [27]. The solution of the gas-phase equations is coupled with those of the liquid-phase equations through the boundary conditions. One notable difference between the quasi-steady and transient formulations is due to the numerical solution of the continuity and momentum equations. In the former, the continuity equation is solved exactly, and the momentum equation is not solved as the pressure is assumed to be uniform.

3. Results and discussion

Results for *n*-heptane droplets evaporating into various nitrogen environments of different thermodynamic states, predicted with the transient (TS) and the quasi-steady (QS) vaporization models, will be presented later in this section. Before these results are presented, the predictions are first validated against the available experimental data for several significant aspects of model performance such as thermophysical properties, vapor–liquid equilibrium and the energy required for phase change at the droplet surface.

Fig. 1(a) shows the predicted Lewis number of *n*-heptane vapor in nitrogen gas at 300 K and the Prandtl

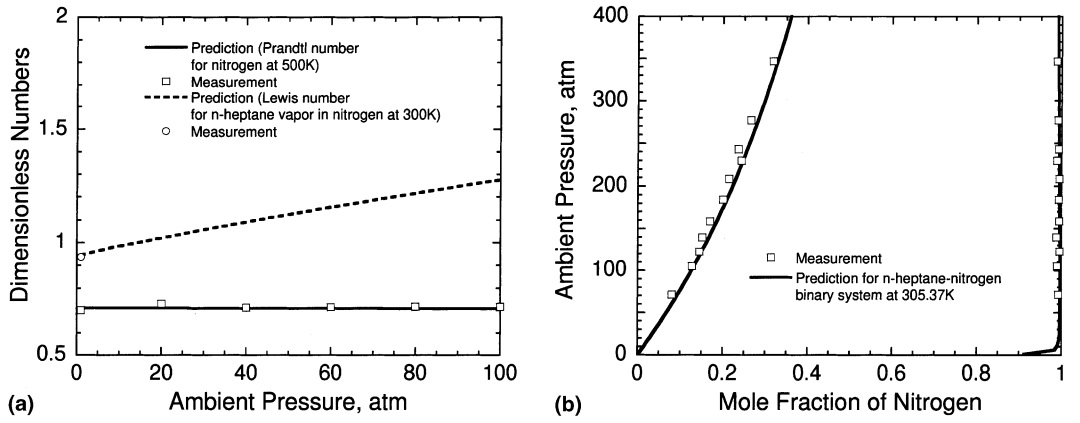

Fig. 1. (a) Comparison of predicted Prandtl number for nitrogen at 500 K and Lewis number for *n*-heptane vapor in nitrogen at 300 K with measurements. The measurements were derived from the measured data of Vargaftik [28]. (b) Mole fraction of nitrogen for a *n*-heptane–nitrogen system in thermodynamic equilibrium at 305.37 K. The measured data is from Knapp [29].

number of nitrogen gas at 500 K together with the corresponding measured values, plotted as functions of pressure. The measurements shown in the figure were derived from the measured data of Vargaftik [28]. The results show that, as the pressure increases, the Prandtl number keeps almost constant, whereas the Lewis number increases and deviates increasingly from unity with increasing pressure. As indicated elsewhere [5,13,14], the accurate prediction of thermophysical properties is important for correctly predicting the vaporization process. The above comparisons indicate that the gas properties are reasonably predicted with the present models for both low and high pressure conditions. Fig. 1(b) presents the predicted phase equilibrium in terms of the variation of nitrogen mole fraction with pressure. A reasonable agreement is also indicated between the predicted and the measured results of Knapp [29]. Other comparisons with experimental data were also made for liquid thermal conductivity, liquid heat capacity, and the energy required for phase-change at the droplet surface. It was found that excellent agreements were generally obtained between the predicted and experimental results for these properties.

Fig. 2 further shows the comparison of predictions of both the TS and QS models for droplet vaporization with corresponding experimental data of Nomura et al. [17]. Results are presented in terms of the temporal variation of non-dimensional surface area for two different ambient conditions. It is evident that the TS model can reproduce the experimental data over a range of pressure and temperature. However, for the present cases, the QS model under-predicts the surface regression rate and thus over-predicts the droplet lifetime, and the amount of underprediction becomes more pronounced for the higher pressure case. The results also

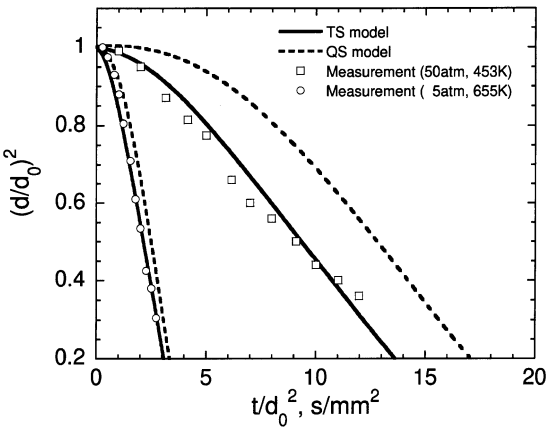

Fig. 2. Comparison of predicted temporal variation of droplet surface area with the measured data of Nomura [17] for two different ambient conditions. Solid line: the transient model. Dashed line: the quasi-steady model.

show that as the pressure increases, the droplet heatup time occupies a more significant part of droplet lifetime since the liquid boiling temperature increases with pressure.

Next, results are then presented using the TS and QS models for *n*-heptane droplets evaporating into an ambience of nitrogen with initial temperature of 300 K. The ambient temperature and pressure range from 500–2000 K and 1–150 atm, respectively. The initial droplet sizes are 0.05–0.5 mm in diameter. These ranges cover the sub- and super-critical environmental states of the *n*-heptane fuel and include the conditions in which practical droplets and sprays evaporate. Since both the TS and QS models are based on the same formulation to calculate the gas- and liquid-transport properties, the

interphase phenomena, and the liquid-phase transient processes, the difference in the predictions of the two models is due to the gas-phase unsteadiness. The results presented in the following, if not mentioned particularly, are for the 0.05 mm droplet.

Fig. 3(a) shows the temporal variation of non-dimensional surface area obtained using the TS and QS models for three different ambient pressures at 500 K. As seen from the figure, the predicted vaporization processes of both models are in good qualitative and quantitative agreement for the atmospheric pressure case. However, as the ambient pressure increases, both the quantitative and the qualitative differences between the two predicted vaporization processes become increasingly more noticeable. For this $T_a = 500$ K case, the QS model generally predicts a smaller initial regression rate, a larger regression rate during the late vaporizing period, and eventually a longer droplet lifetime. These disparities increase with pressure, and become quite significant at high pressures (e.g., see $p = 70$ atm case).

In order to explain the above behavior, consider the unsteadiness of the transient vaporization process predicted with the TS model. Let τ_g and τ_s denote the characteristic time scales for gas-phase unsteady diffusion and for droplet surface heating, respectively. Then reasonable expressions for these time scales are given by:

$$\tau_g = \frac{r_s^2}{\alpha}, \quad \tau_s = \frac{T_b - T_0}{dT_s/dt}, \tag{19}$$

where α is the gas thermal diffusivity, T_0 the droplet initial temperature and T_b is the normal boiling temperature of the liquid fuel (an alternative for this quantity can also be the critical temperature of the fuel for high-pressure vaporization). Thus, the time scale ratio $R_T = \tau_g/\tau_s$ can be regarded as a measure of the gas-phase unsteadiness. Similarly, if we define:

$$\tau'_g = \frac{r_s^2}{D_l}, \quad \tau'_s = \frac{1}{dY_s/dt}, \tag{20}$$

then the time scale ratio $R_f = \tau'_g/\tau'_s$ can be another form of the measure of the gas-phase unsteadiness, where D_l is the fuel vapor diffusivity and Y_s the fuel vapor concentration at the droplet surface. For unity Lewis number and ideal phase-change at the droplet surface, as assumed for classical low-pressure models [1–3,6], both measures are very close. However, for high-pressure conditions both measures deviate from each other increasingly with increasing pressure and temperature, as will be seen later.

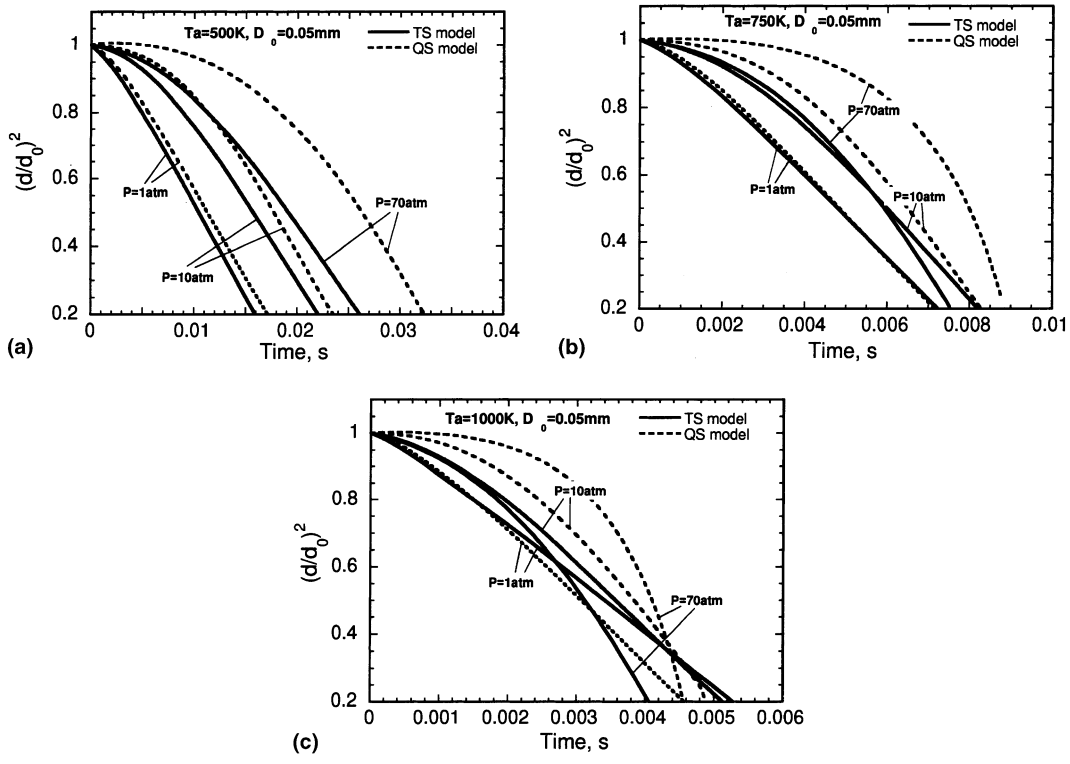

Fig. 3. Temporal variation of droplet surface area for three different ambient pressures 1, 10, and 70 atm at: (a) 500 K, (b) 750 K, and (c) 1000 K. The initial diameter is 0.05 mm. Solid line: the transient model. Dashed line: the quasi-steady model.

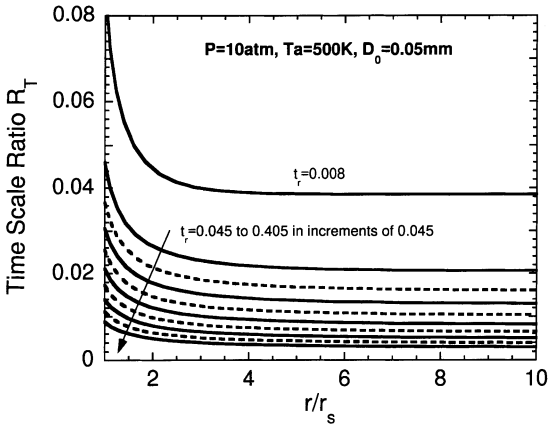

Fig. 4. Time- and space-distribution of gas-phase unsteadiness for droplet vaporization process at 10 atm and 500 K. The initial diameter is 0.05 mm. t_r is the time normalized by the droplet lifetime. The unsteadiness is expressed in terms of R_T which is the time scale ratio of the characteristic time of gas-phase thermal diffusion to that of droplet heating.

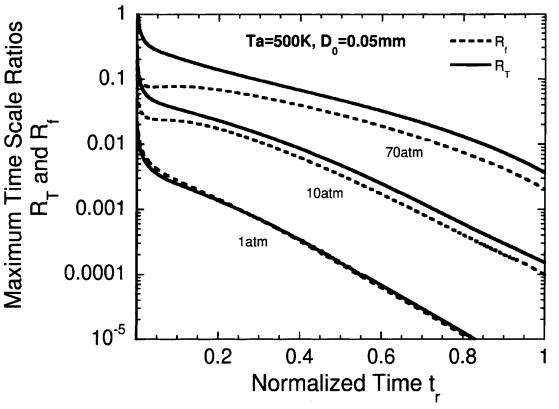

Fig. 5. Temporal variation of the maximum gas-phase unsteadiness in terms of time scale ratios R_T and R_f for three different pressures 1, 10, 70 atm at 500 K. The initial diameter is 0.05 mm. t_r is the time normalized by the droplet lifetime. R_f is the time scale ratio of the characteristic time of gas-phase mass diffusion to that of phase change. See Fig. 4 for the definition of R_T.

Fig. 4 shows the evolution of the gas-phase unsteadiness, measured in terms of the time scale ratio R_T, with time for the 10 atm case of Fig. 3(a), where the quantity t_r is the time normalized by the corresponding droplet lifetime. At a certain moment, the gas-phase unsteadiness is seen to attain a maximum value in the region next to the droplet liquid surface, then decreases rapidly to a value which is almost constant at large radial locations. The rapid spatial variation in the unsteadiness is limited to a narrow region near the droplet surface that is generally within 4 droplet radii. As the vaporization process evolves, the unsteadiness decreases sharply at first and then gradually. Further calculations indicate that the characteristics of the unsteadiness shown in Fig. 4 hold qualitatively for other cases at different ambient pressures and/or different temperatures, but they are quantitatively different.

Fig. 5 shows the variation of the maximum gas-phase unsteadiness (i.e., in the region next to the droplet surface) with normalized time for the same three cases of Fig. 3(a), where the unsteadiness is expressed in terms of the time scale ratios R_T and R_f. As shown in the figure, the ambient pressure significantly affects the gas-phase unsteadiness. The changes in time scale ratios (or in gas-phase unsteadiness) are approximately of the same order as the pressure ratio. (In fact, as will be indicated in Fig. 12(a), the overall gas-phase unsteadiness of this case is inversely proportional to the ambient pressure). With increasing pressure, the part of the droplet lifetime that can be regarded as being in the quasi-steady state obviously decreases. For example, as seen from this figure, if it is assumed that the quasi-steady state is attained when the time scale ratio is of order $O(10^{-3})$, then the quasi-steady vaporization process lasts for about 75% of the droplet lifetime for the 1 atm case, 25% for the 10 atm case, whereas for the 70 atm case the unsteady process persists for all of the droplet lifetime. The disparities between both time scale ratios also increase with ambient pressures. This is mainly due to the fact that the Lewis number of the vaporization process deviates increasingly from unity with increasing pressure, as shown in Fig. 1(a), and that a more nonlinear relation occurs between the phase equilibrium concentration and temperature at higher pressures.

Figs. 6(a) and (b) present the radial distributions of gas temperature and fuel vapor concentration predicted with the TS model, for the same 10 atm case shown in Figs. 3(a), 4, and 5. A feature of the evolution process is that rapid spatial evolution and strong transients exist during the early period of the vaporization process (see the process before time 0.222). The vapor concentration process evolves more gradually and never reaches a steady state. Figs. 7(a) and (b) present the predicted vaporization process using the QS model for the same case, which, as seen from the figures, is intrinsically different from the TS predictions. During the initial period the significant gas-phase unsteadiness causes large differences between the both models. The QS model results in smaller heat and mass fluxes at the droplet surface, since it predicts much smaller temperature and fuel vapor gradients during this period, as shown in Figs. 8(a) and (b). Correspondingly, the QS model predicts lower droplet surface temperatures and fuel vapor concentrations (compare Figs. 6(a),(b) and 7(a),(b) for $r/r_s = 1$) and a smaller regression rate (see Fig. 3). After the initial period, the gas-phase

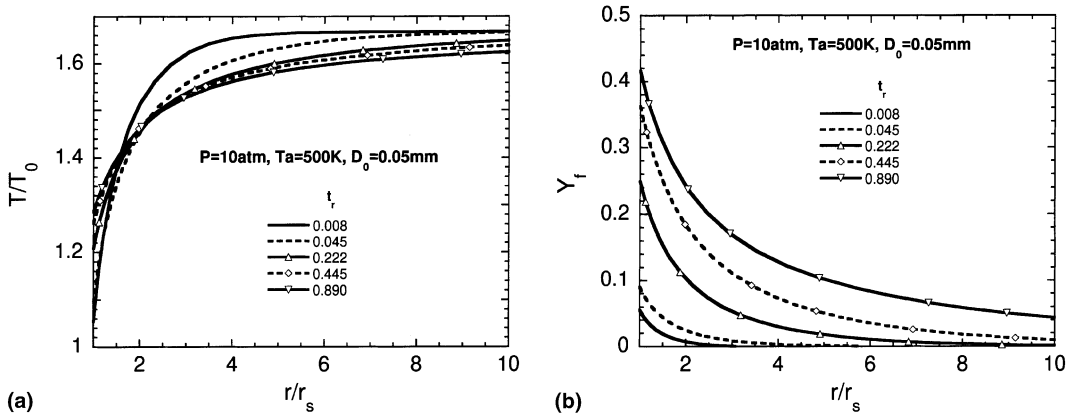

Fig. 6. Radial distributions of gas-phase parameters for the vaporization process at 10 atm and 500 K, predicted by the transient model: (a) gas temperature normalized by the initial droplet temperature, and (b) fuel vapor concentration.

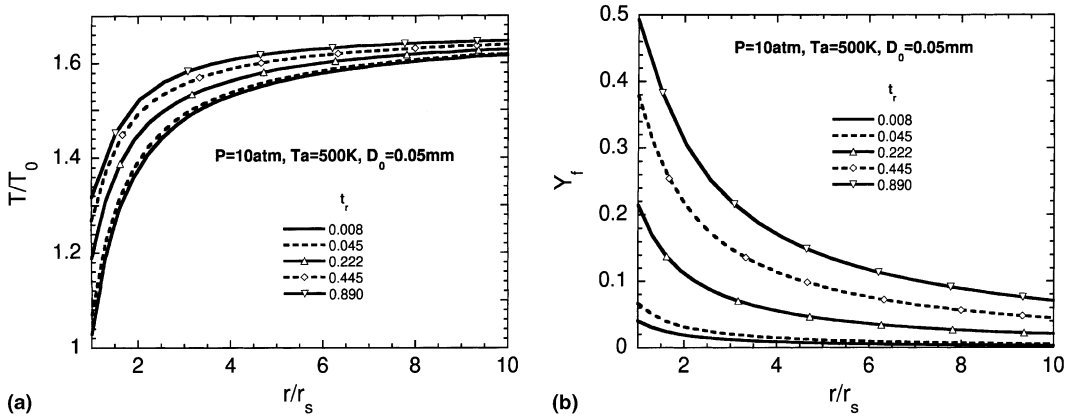

Fig. 7. Radial distributions of gas-phase parameters for the vaporization process at 10 atm and 500 K, predicted by the quasi-steady model: (a) gas temperature normalized by the initial droplet temperature, and (b) fuel vapor concentration.

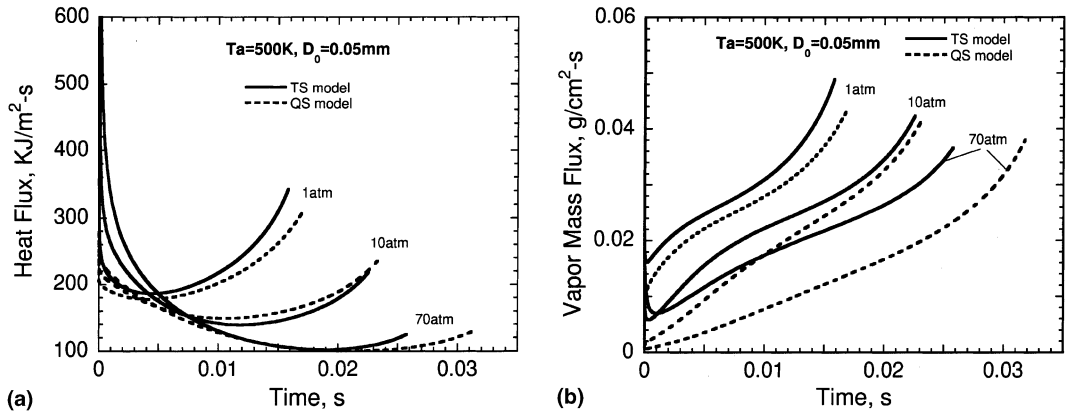

Fig. 8. Temporal variation of: (a) heat flux, and (b) vapor mass flux at droplet surface for vaporization processes for three different pressures 1, 10, and 70 atm at 500 K. Solid line: the transient model. Dashed line: the quasi-steady model.

unsteadiness greatly decreases, and the difference between both predictions decreases (see Fig. 8(a)). However, the QS model, which implies infinite gas-phase transport rate, transmits the ambient energy to the droplet surface and diffuses the vapor mass away from the droplet more rapidly. It thus results in a higher surface temperature and a higher fuel vapor concentration after a certain time (also compare Figs. 6(a),(b) and 7(a),(b) for $r/r_s = 1$), and eventually, results in a larger regression rate (see Fig. 3). As the ambient pressure increases, owing to the significant change in gas-phase unsteadiness (see Fig. 5), the quantitative differences between the predicted parameter radial distributions of both models increase. As seen in Figs. 8(a) and (b), the differences between the predicted mass and heat fluxes at the droplet surface of both models subsequently increase. As a consequence, the difference between the vaporization processes predicted with the TS and QS models increases, as indicated in Fig. 3.

An interesting result is that the ambient temperature also has a significant influence on the unsteadiness of the vaporization process, which is not emphasized adequately in previous studies. This can be clearly seen from Fig. 9, where the gas-phase unsteadiness are presented in terms of the ratios R_T and R_f for the three different ambient temperatures at 10 atm. In fact, the influence of ambient temperature on gas-phase unsteadiness is even larger than that of the ambient pressure. For example, the unsteadiness of the 1000 K case is about one order of magnitude larger than that of the 500 K case, although the temperature of the former is only doubled. The difference between both the time scale ratios also increases with temperature mainly because of the increase in the deviation of the Lewis number from unity.

Figs. 3(b) and (c), along with Fig. 3(a) analyzed above, further show the influence of the ambient temperature on the vaporization processes. As compared to the predictions of the TS model, the characteristics of the vaporization process predicted with the QS model, e.g., the smaller early regression rate and the larger late regression rate, are magnified by increasing the ambient temperature. To explain this, Figs. 10(a) and (b) present the heat and mass fluxes at the droplet surface for the three different pressures at 750 K. Compared to the 500 K case for the same pressure shown in Figs. 8(a) and (b), the increased ambient temperature demonstrates greatly increased heat and mass fluxes at the droplet surface for the TS model and for the early period of the vaporization process. This is because the larger gas-phase unsteadiness and stronger transients occur for the higher ambient temperature, and thus, result in a more obvious increase in the early regression rate predicted by the TS model. On the other hand, at higher ambient

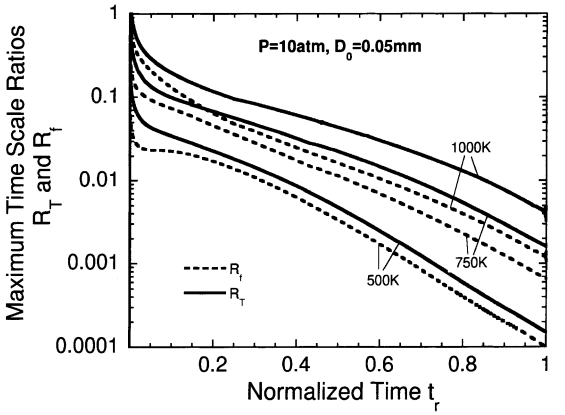

Fig. 9. Temporal variation of the maximum gas-phase unsteadiness in terms of time scale ratios R_T and R_f for three different temperatures 500, 750, and 1000 K at 10 atm. The initial droplet diameter is 0.05 mm. t_r is the time normalized by the droplet lifetime. See Fig. 5 for the definitions of R_T and R_f.

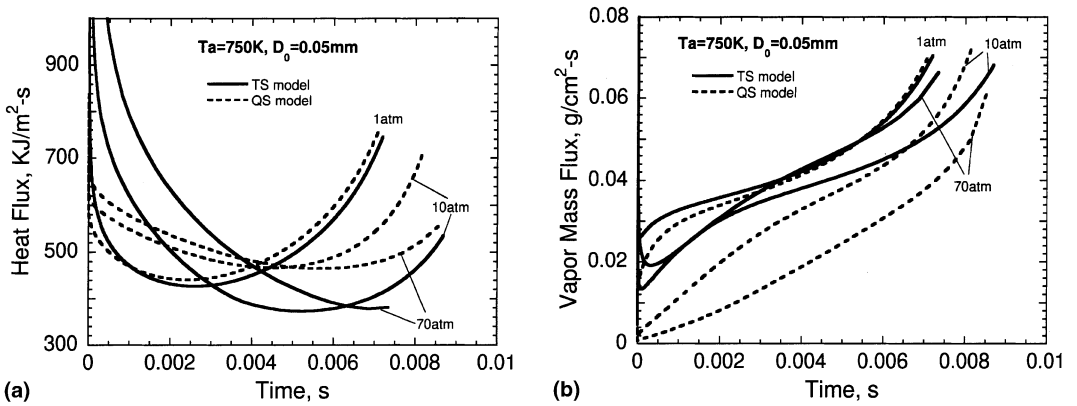

Fig. 10. Temporal variation of: (a) heat flux, and (b) vapor mass flux at droplet surface for vaporization processes for three different pressures 1, 10, and 70 atm at 750 K. Solid line: the transient model. Dashed line: the quasi-steady model.

temperatures, the QS model predicts more energy transferred to the droplet surface and this, in turn, gives larger heat and mass fluxes which, as seen in Figs. 10(a) and (b), eventually exceed the corresponding values of the TS model. Therefore, the QS model produces a larger regression rate during the late vaporization period. Correspondingly, the difference between the predicted vaporization processes of both models increases with ambient temperature.

The above changes in the predicted regression rates also add complexity to the predicted droplet lifetimes of both models. This can be seen from Figs. 10(a) and (b) which show that the lower the ambient pressure, the earlier the predicted heat and mass fluxes of the QS model exceed those of the TS model. As a result, the predicted regression rate of QS model begins to be larger than that of the TS model earlier (see Figs. 3(a)–(c)). Therefore, it is more likely that the predicted droplet lifetime of the QS model of the lower pressure case begins to become shorter than that of the TS model. This is clearly reflected in Figs. 3(a)–(c). For example, as the ambient temperature increases from 500 to 750 K, the predicted lifetime of the QS model at 1 atm first becomes smaller than that of the TS model, whereas only after the temperature further increases to 1000 K, are the results similar to those for the 10 atm case. Additional calculations were performed to assess the influence of the environment on the TS and QS model predictions. It was found that the QS model qualitatively predicts the same trends of droplet lifetime at different ambient pressures and temperatures as those predicted with the TS model.

In Fig. 11, the temporal variation of the vaporization constant is shown at different pressures for the QS and TS models. Here only the results for the cases shown in Fig. 3(a) are presented. The vaporization constant is defined as $-\mathrm{d}(d^2)/\mathrm{d}t$. In previous experimental and theoretical investigations, such plots are often used to quantify deviations from the classical d^2-law behavior. As shown by the predictions of the TS model, the higher the ambient pressure, the shorter the period the d^2-law holds, and at a high enough pressure, the period that follows the d^2-law vanishes. This is a conclusion that has been validated both experimentally and theoretically by many researchers [5]. This also indicates the reliability of the present TS model. At atmospheric pressure, the QS model also predicts d^2-law behavior after the initial droplet heat-up phase. However, it is interesting to note that the QS model does not predict the d^2-law behavior at high pressures. Considering that the d^2-law is derived under the assumptions of gas-phase quasi-steadiness and constant properties, the reason that the QS model does not predict the d^2-law behavior is because of the temperature–pressure-composition-dependent thermophysical and phase change properties considered in the present QS model. This emphasizes the need to use a transient model for high-pressure predictions.

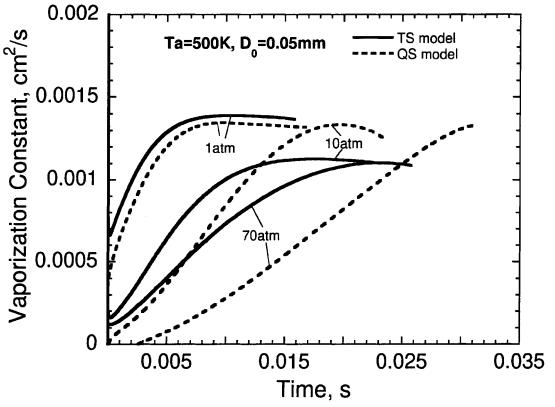

Fig. 11. Temporal variation of vaporization constant for the same cases of Fig. 3(a). The vaporization constant is defined as $-\mathrm{d}(d^2)/\mathrm{d}t$. Solid line: the transient model. Dashed line: the quasi-steady model.

Further results characterizing the gas-phase unsteadiness are presented in Figs. 12(a) and (b). Here the time scale ratio is defined as the ratio of the droplet-surface-area-averaged diffusion time to the droplet lifetime. The former is defined as r_s^2/D_s, a characteristic time of the gas-phase diffusion process, where r_s is droplet radius and D_s the coefficient of gas diffusion in the region near the droplet surface. The time scale ratio can be regarded as a measure of gas-phase unsteadiness for the overall vaporization process. As seen from Fig. 12(a), the unsteadiness increases with pressure nearly linearly at low ambient temperatures, and acceleratively at high ambient temperatures. The influence of temperature is presented in Fig. 12(b). Increasing the ambient temperature enhances the gas-phase diffusion process and thus reduces the unsteadiness. However, the increase in process transients competes with the above factor, and as seen in the figure, the unsteadiness increases with temperature, at a more pronounced rate at higher pressures and at lower ambient temperatures.

Studies were also conducted for the droplet with initial diameter of 0.5 mm. Qualitatively similar results as those for the 0.05 mm droplet shown above were obtained. However, for the larger droplet, it is possible for the droplet surface to reach the critical mixing state before it fully vaporizes. Fig. 13 shows the minimum critical ambient pressure as a function of ambient temperature, predicted with both the TS and QS models. In order to obtain the minimum pressure value at a fixed ambient temperature, simulations were performed with increasingly higher pressures until the critical mixing state was observed at the droplet sur-

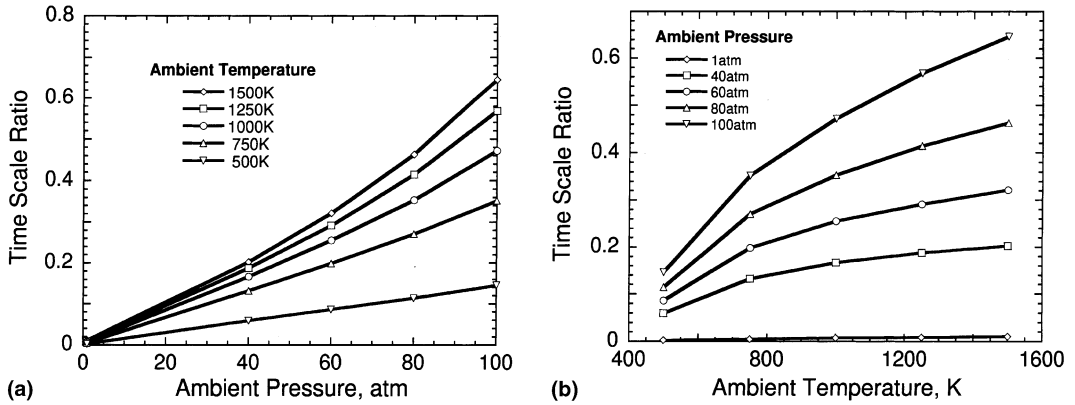

Fig. 12. Variation of gas-phase unsteadiness of overall vaporization process: (a) with ambient pressure at different ambient temperatures, and (b) with ambient temperature at different ambient pressures. Gas-phase steadiness is defined as the ratio of the characteristics time of gas mass diffusion near the droplet surface to the droplet lifetime. The droplet initial diameter is 0.05 mm.

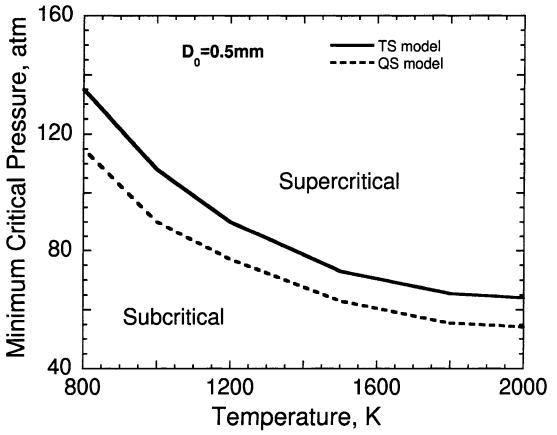

Fig. 13. Minimum pressure, required for a *n*-heptane fuel droplet to attain the critical mixing state, plotted as a function of ambient temperature. The droplet initial diameter is 0.5 mm. Solid line: the transient model. Dashed line: the quasi-steady model. (The critical pressure and temperature of pure *n*-heptane are 27.0 atm and 540.3 K, respectively.)

face. As seen from the figure, the QS model predicts a vaporization process which reaches the critical mixing state at a significantly lower ambient pressure. This implies that the vaporization process of the QS model reaches the critical mixing state earlier than that of the TS model. The plots in Fig. 13 also represent boundaries, predicted with both models in terms of the ambient temperature and pressure, between the sub- and super-critical vaporization states. Any point above the curve indicates that a critical mixing state will be reached sometime during the droplet lifetime, i.e., the droplet will undergo transcritical evaporation during its lifetime. On the other hand, any point below the curve implies that the droplet is not expected to attain a supercritical state during its lifetime. Also, the farther a point is from the curve in the supercritical region, the earlier in its lifetime the droplet is expected to attain the critical mixing state.

4. Conclusions

Two comprehensive high-pressure droplet vaporization models, namely a transient model and a model assuming gas-phase quasi-steadiness, have been presented. Except for the quasi-steady assumption for the second model, these models incorporate all high-pressure effects and consider the transient liquid-phase transport within droplet interior. The accuracy of both models is examined with available experimental data in terms of predictions of the thermophysical properties, the phase change process at the droplet surface, and the droplet vaporization processes. It was found that the predictions of the transient model agree very well with all the experimental data examined.

Both models were employed to investigate high-pressure vaporization of single droplets of different initial sizes for a wide range of ambient pressures and temperatures. Based on the predictions and comparisons of the models, the following conclusions are reached: (1) Strong gas-phase unsteadiness exists during the early period of the vaporization process. The unsteadiness attains a maximum value in the gas near the droplet surface and decreases rapidly to an almost constant value at large radial locations. These characteristics apply for the range of ambient pressures and/or temperatures considered. (2) Gas-phase unsteadiness increases with pressure linearly at low ambient temperature and acceleratively at high ambient

temperature. Gas-phase unsteadiness generally increases with temperature, and at a more pronounced rate for higher pressures and/or for lower ambient temperatures. The influence of the ambient temperature on gas-phase unsteadiness is stronger than that of the ambient pressure. (3) Compared to the transient model, the quasi-steady model predicts a smaller regression rate initially and a larger regression rate during the later period of the droplet lifetime. This is mainly because it predicts a significantly different evolution process of the radial distribution of gas temperature, and results in smaller and larger heat and mass fluxes at the droplet surface during the early and late periods, respectively. (4) The differences between the predicted regression rates are magnified with increasing ambient temperatures and/or pressures. The difference between the predicted vaporization processes of both models thus increases with the ambient parameters. These characteristics add complexity to the predicted droplet lifetimes of both models. (5) The above conclusions also apply for the vaporization processes of droplets of different initial sizes. The vaporization process predicted with the quasi-steady model reaches the critical mixing state earlier than that predicted with the transient model.

Acknowledgements

The authors thank Caterpillar and the DOE/Sandia Laboratories for supporting this work.

References

[1] A. Williams, Combustion of droplet of liquid fuels: a review, Combust. Flame 21 (1973) 1–31.
[2] C.K. Law, Recent advances in droplet vaporization and combustion, Prog. Energy Combust. Sci. 8 (1982) l71–201.
[3] W.A. Sirignano, Fuel droplet vaporization and spray combustion, Prog. Energy Combust. Sci. 9 (1983) 291–322.
[4] F. Peng, S.K. Aggarwal, A review of droplet dynamics and vaporization modeling for engineering calculations, ASME J. Eng. Gas Turbines Power 117 (1995) 453–461.
[5] S.D. Givler, J. Abraham, Supercritical droplet vaporization and combustion studies, Prog. Energy Combust. Sci. 22 (1996) 1–28.
[6] G.A.E. Godsave, Studies of the combustion of drops in a fuel spray – the burning of single drops of fuel, in: Proceedings of the Fourth Symposium (International) on Combustion, Williams and Wilkins, Baltimore, 1953, pp. 818–830.
[7] B. Abramzon, W.A. Sirignano, Droplet vaporization model for spray combustion calculations, Int. J. Heat Mass Transfer 32 (1989) 1605–1618.
[8] E.W. Curtis, A. Ulodogan, R.D. Reitz, A new high pressure droplet vaporization model for diesel engine modeling, SAE952431, 1995.
[9] A.A. Amsden, KIVA-3V: A block-structured KIVA program for engines with vertical or canted valves, LA-13313-MS, 1997.
[10] C.K. Law, S.H. Chung, N. Srinivasan, Gas-phase quasi-steadiness and fuel vapor accumulation effects in droplet burning, Combust. Flame 38 (1980) 173–198.
[11] M. Matalon, C.K. Law, Gas-phase transient diffusion in droplet vaporization and combustion, Combust. Sci. 50 (1983) 219–229.
[12] S.C. Wong, T.S. Hsu, J.C. Chang, Validity of droplet ignition criteria derived assuming gas-phase quasisteadiness, J. Propulsion Power 11 (1) (1996) 18–25.
[13] H. Jia, G. Gogos, High pressure droplet vaporization; effects of liquid gas solubility, Int. J. Heat Mass Transfer 36 (1993) 4419–4431.
[14] G.S. Zhu, S.K. Aggarwal, Transient supercritical droplet vaporization with emphasis on the effects of equation of state, Int. J. Heat Mass Transfer 43 (2000) 1157–1171.
[15] J. Stengele, H.J. Bauer, S. Wittig, Experimental and theoretical study of droplet vaporization in a high pressure environment, ASME paper 96-GT-442, 1996.
[16] R.C. Reid, J.M. Prausnitz, B.E. Poling, The Properties of Gases and Liquids, 4th ed., McGraw-Hill, New York, 1987, pp. 29–94.
[17] H. Nomura, Y. Ujiie, H.J. Rath, J. Sato, M. Kono, Experimental study of high-pressure droplet evaporation using microgravity conditions, in: Proceedings of the 26th Symposium (International) on Combustion, The Combustion Institute, 1996, pp.1267–1273.
[18] T.H. Chung, M. Ajlan, L.L. Lee, K.E. Starling, Generalized multiparameter correlation for nonpolar and polar fluid transport properties, Ind. Eng. Chem. Res. 27 (1988) 671–679.
[19] T.H. Chung, L.L. Lee, K.E. Starling, Applications of kinetic gas theories and multiparameter correlation for prediction of dilute gas viscosity and thermal conductivity, Ind. Eng. Chem. Fundam. 23 (1984) 8–13.
[20] P.D. Neufeld, A.R. Janzen, R.A. Aziz, Empirical equations to calculate 16 of the transport collision integrals $\Omega^{l,s}$ for the Lennard–Jones potential, J. Chem. Phys. 57 (1972) 1100–1102.
[21] S. Takahashi, Preparation of a generalized chart for the diffusion coefficients of gases at high pressures, J. Chem. Eng. Jpn. 6 (1974) 417–420.
[22] R.B. Bird, W.E. Stewart, E.N. Lightfoot, in: Transport Phenomena, Wiley, New York, 1960.
[23] I.L. Byung, G.K. Michael, A generalized thermodynamic correlation based on three-parameter corresponding states, J. AIChE 21 (1975) 510–527.
[24] L.P. Filippov, Thermal conduction of solutions in associated liquids: thermal conduction of 50 organic liquids, Chem. Abstr. 49 (1955) 15430–15431.
[25] L.P. Filippov, Thermal conduction of solutions in associated liquids: thermal conduction of 50 organic liquids, Chem. Abstr. 50 (1956) 8276.
[26] K. Nakanishi, Prediction of diffusion coefficients of non-electrolytes in dilute solution based on generalized Hammond–Strokes plot, Ind. Eng. Chem. Fundam. 17 (1978) 253–256.

[27] S.V. Patankar, in: Numerical Heat Transfer and Fluid Flow, McGraw-Hill, New York, 1980, p. 52.
[28] N.B. Vargaftik, Handbook of Physical Properties of Liquids and Gases, Hemisphere Publishing Corporation, 1975, pp. 433–463, 634–636.
[29] H. Knapp, R. Doring, L. Oellrich, U. Plocker, J.M. Prausnitz, Vapor–liquid equilibria for mixture of low boiling substances, Chem. Eng. Data Ser., vol. VI, DECHEMA, Frankfurt, 1982.